BNL-102241-2014-TECH
RHIC/AP/135;BNL-102241-2013-IR

Interaction Region Closed Orbits

S. Peggs

December 1999

Collider Accelerator Department
Brookhaven National Laboratory

U.S. Department of Energy
USDOE Office of Science (SC)

DISCLAIMER

RHIC/AP/135
December 11, 1997

Interaction Region Closed Orbits

S. Peggs, V. Ptitsin, S. Tepikian, P. Thompson, D. Trbojevic

Contents

1 Crossing angles

If a *total* crossing angle of α is required, then the absolute bend angles of DX and D0, $\theta_X(\alpha)$ and $\theta_0(\alpha)$, need to be adjusted so that the closed orbit perturbation is localized between the two outer D0 magnets. Localization is guaranteed (to a very good approximation) as the crossing angle is varied if [1]

$$\theta_X(\alpha) = \theta_X(0) - \frac{\alpha}{2}\frac{s_0}{s_0 - s_X} = 18.861 - 1.047\,\alpha \quad \text{[mrad]} \qquad (1)$$

$$\theta_0(\alpha) = \theta_0(0) - \frac{\alpha}{2}\frac{s_X}{s_0 - s_X} = 15.186 - 0.547\,\alpha \quad \text{[mrad]} \qquad (2)$$

where s_X and s_0 are the bending center locations listed in Table 1. Note that the absolute bend angles and fields decrease with increasing crossing angle.

Quantity	Symbol	Units	DX	D0
Magnetic length		[m]	3.70	3.60
Bending radius		[m]	196.17	237.06
Bend angle	θ	[mrad]	18.86	15.19
Bend center (from IP)	s	[m]	11.65	22.30
Bend "leverage"	$s\theta$	[m]	0.2197	0.3387

Table 1: DX and D0 dipole parameters, when the crossing angle is zero. Bend center locations are measured in meters from the IP.

Although the DX magnet has a coil ID of 180 mm, the available bore radius is only 69.85 mm due to the presence of the warm vacuum pipe. The maximum crossing angle at the IP is limited by the aperture at the D0 end of the DX dipole, at a distance $s_{end} = 13.76$ m from the IP, as shown in Fig. 1. For example, a crossing angle of $\alpha = 1$ mrad moves each beam approximately $s_{end}\alpha/2 = 6.88$ mm closer to the vacuum pipe. This is to be compared with the beam size of $\sigma = 3.42$ mm that applies when $\beta_{end} = 190$ m in $\beta^* = 1$ m optics with a gold beam emittance of 40 π mm mrad at top energy.

The physical aperture of the triplet quadrupoles also constrains the beam, when the maximum beta β_{max} in the triplet is large in low β^* optics. For example, $\beta_{max} = 1354$ m when $\beta^* = 1$ m, resulting in a physical aperture in the triplet of $\pm 6.2\sigma$. If the same aperture of $\pm 6.2\sigma$ is used as a limiting factor at the end of the DX magnet, the maximum possible crossing angle is $\alpha_{max} = 2\phi_2 = 1.31$ mrad, as drawn in Fig. 1.

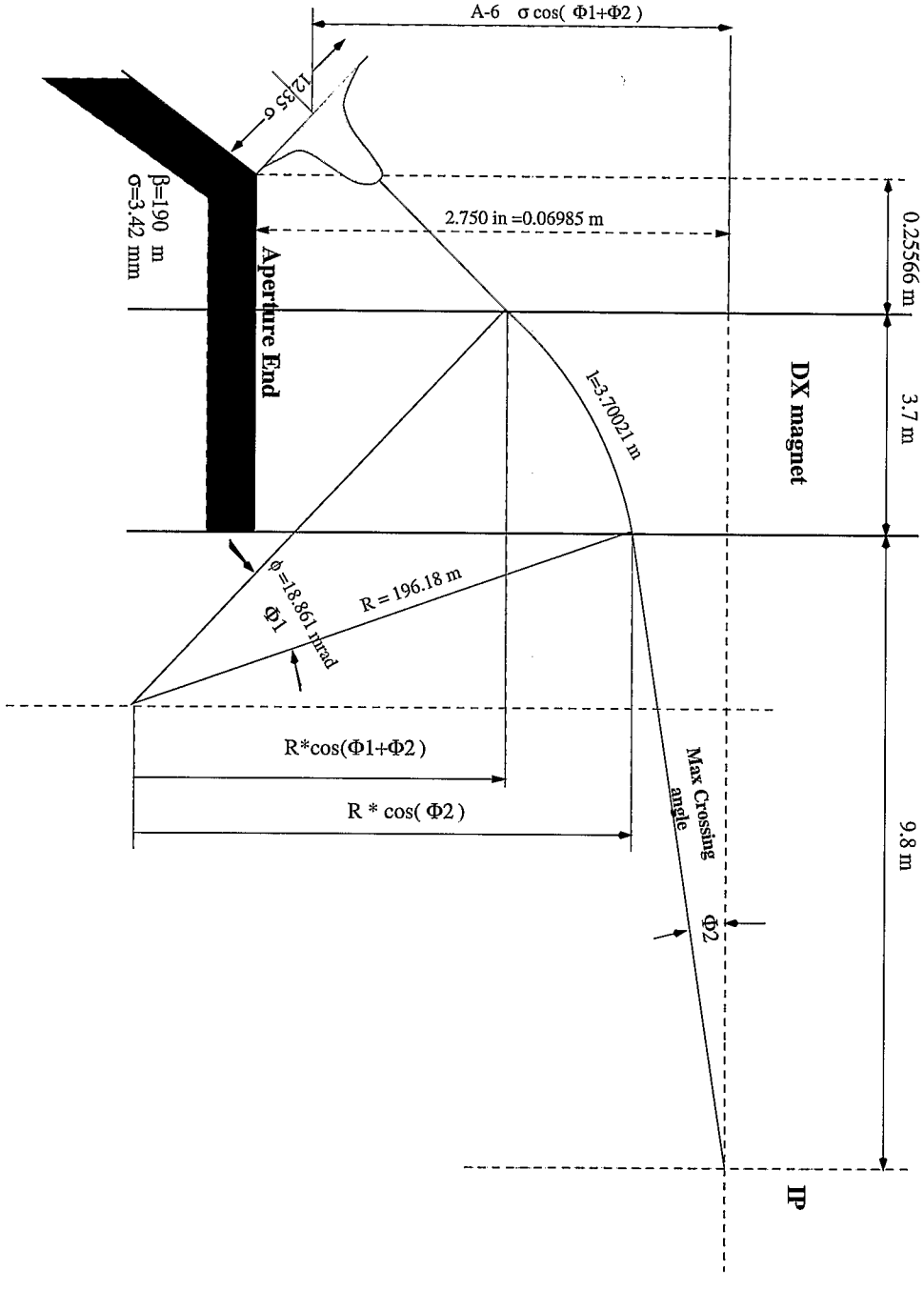

Figure 1: Maximum crossing angle defined by the limiting aperture at the end of the DX magnet.

In practice the amount of DX aperture available for use by a non-zero crossing angle will vary with emittance, β^*, energy, and ion species [2]. Also, it can be argued that the maximum crossing angle derived in the previous paragraph is a lower bound, since the "equal aperture" assumption is rather conservative - beam is much more sensitive to field errors in the triplet quadrupoles (where the β values are much higher) than at the end of DX. It may therefore prove possible to decrease the DX field by 10% or more. Since the DX magnets may well limit RHIC performance, this could translate into the possibility of increasing the top energy by 10%.

1.1 "Gold" and "brass" DX magnets

Assuming that DX magnets limit the maximum operating energy, it is desirable to locate the weakest "brass" magnets near IPs where crossing angles are allowed, placing "gold" magnets where the total angle α must be kept zero. The decision to label a DX magnet "gold" also depends partly on its field quality performance. Table 2 classifies the IPs from these perspectives.

IP	Contents	$\beta^*[m]$	G/B	Comments
2	BRAHMS	2	B	
4	RF	10	G	Center beam in 200 MHz cavities
6	STAR	$1 \rightarrow 2$	G	
8	PHENIX	$1 \rightarrow 2$	G	
10	PHOBOS	$2 \rightarrow 5$	B	Abort aperture: 51×76 mm near Q3
12	vacant	10	B	

Table 2: Classification of IPs by their need or tolerance for "Gold" (G) or "Brass" (B) DX magnets.

The BRAHMS experiment at 2:00 can operate with a non-zero crossing angle, and will be run with a modest value of $\beta^* \approx 2$ m, allowing the allocation of "brass" DX magnets. Synchrobetatron resonances may be generated if the beams do not pass through the center of the common 200 MHz RF cavities, which are located at the 4:00 straight. This leads to the need for zero crossing angle, and "gold" DX magnets. Operation with zero crossing angle and with the lowest possible beta value ($\beta^* \approx 1$ m) is foreseen at the major experiments, STAR and PHENIX, requiring "gold" DX magnets. The extraction kickers of the abort system are close to the Q3 magnets on either side of the PHOBOS experiment. These kickers have a full aperture of 51×76 mm, which only allows β^* to be reduced to about 2 m. This, and the fact that PHOBOS can sustain

a non-zero crossing angle, allows the DX magnets at 10:00 to be "brass".

1.2 Unequal species

When unequal species collide it is usually assumed that Blue and Yellow beams have identical speeds, so that synchronized beams go down the center of the beam tubes in the arcs [3]. Table 3 lists the angular strengths of DX and D0 magnets for various combinations of equal speed species [4].

2 Common mode DX and D0 errors

In general, a dipole error $\Delta x'$ at a *single* DX or D0 magnet generates a closed orbit perturbation wave

$$x(s) \;=\; \Delta x' \sqrt{\beta_D \beta(s)}\, \frac{\cos(|\Delta\phi| - \pi Q)}{2\sin(\pi Q)} \tag{3}$$

where β_D is the beta function at the dipole, $\Delta\phi$ is the phase advance from the dipole to the observation point s, and Q is the tune. Differentiating with respect to s, and assuming for convenience that $\alpha(s) = 0$, the angular closed orbit perturbation is found to be

$$x' \;=\; \pm\, \Delta x' \sqrt{\frac{\beta_D}{\beta}}\, \frac{\sin(\pi Q - |\Delta\phi|)}{2\sin(\pi Q)} \tag{4}$$

where the positive sign holds if $\Delta\phi > 0$, and vice versa. For example, the angular error at the nearby IP is

$$x'^{*} \;\approx\; \mp\, \Delta x' \sqrt{\frac{\beta_D}{\beta^*}}\, \frac{\cot(\pi Q)}{2} \tag{5}$$

since $\Delta\phi \approx \pi/2$. The minus sign applies if the dipole error precedes the IP in s.

Pairs of dipole errors are more relevant to the present discussion, since there is a common shunt power supply across each pair of DX or D0 magnets at all the IPs except 10:00 (where there is one shunt per dipole) [5]. This arrangement, illustrated in Figure 2, allows the crossing angle to be varied in accordance with equations 1 and 2. It is important to note that *only a local angle bump is possible using DX and D0 shunt power supplies.* A local displacement bump - moving the collision point transversely - requires the use of IR dipole correctors. When the transfer function of a pair of insertion dipoles has an average error (perhaps due to hysteresis), when there is shunt power supply noise, or when the shunt supplies are simply not set correctly, a significant closed orbit wave can circulate.

Blue species	Yellow species	D0(Blue) [mrad]	D0(Yellow) [mrad]	DX(Blue) [mrad]	DX(Yellow) [mrad]
same	same	15.186252	15.186252	18.860790	18.860790
p	d	18.468090	11.904159	25.143578	12.577749
p	O	18.435882	11.936373	25.081917	12.639416
p	Si	18.433658	11.938597	25.077659	12.643674
p	Cu	18.790474	11.581723	25.760766	11.960509
p	I	19.202725	11.169399	26.550002	11.171199
p	Au	19.367477	11.004615	26.865414	10.855755
d	p	11.904159	18.468090	12.577749	25.143578
d	O	15.150063	15.222440	18.791512	18.930068
d	Si	15.147568	15.224935	18.786735	18.934846
d	Cu	15.553416	14.819084	19.563682	18.157895
d	I	16.036428	14.336058	20.488355	17.233209
d	Au	16.233847	14.138631	20.866293	16.855262
O	p	11.936373	18.435882	12.639416	25.081917
O	d	15.222440	15.150063	18.930068	18.791512
O	Si	15.183756	15.188747	18.856013	18.865568
O	Cu	15.589549	14.782951	19.632854	18.088723
O	I	16.072335	14.300150	20.557095	17.164468
O	Au	16.269611	14.102865	20.934760	16.786793
Si	p	11.938597	18.433658	12.643674	25.077659
Si	d	15.224935	15.147568	18.934846	18.786735
Si	O	15.188747	15.183756	18.865568	18.856013
Si	Cu	15.592040	14.780459	19.637623	18.083953
Si	I	16.074810	14.297675	20.561833	17.159729
Si	Au	16.272076	14.100399	20.939479	16.782074
Cu	p	11.581723	18.790474	11.960509	25.760766
Cu	d	14.819084	15.553416	18.157895	19.563682
Cu	O	14.782951	15.589549	18.088723	19.632854
Cu	Si	14.780459	15.592040	18.083953	19.637623
Cu	I	15.670827	14.701671	19.788451	17.933124
Cu	Au	15.869396	14.503096	20.168591	17.552979
Au	p	11.004615	19.367477	10.855755	26.865414
Au	d	14.138631	16.233847	16.855262	20.866293
Au	O	14.102865	16.269611	16.786793	20.934760
Au	Si	14.100399	16.272076	16.782074	20.939479
Au	Cu	14.503096	15.869396	17.552979	20.168591
Au	I	14.986999	15.385503	18.479347	19.242233

Table 3: DX and D0 angles for various equal speed species, with zero crossing angle.

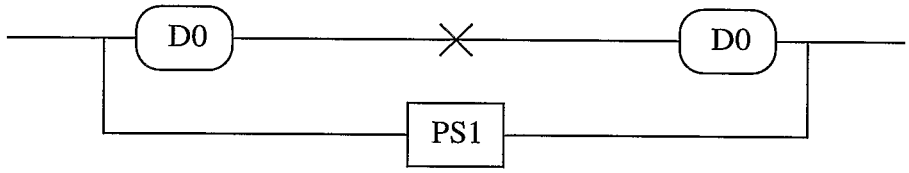

YELLOW ring D0 shunt

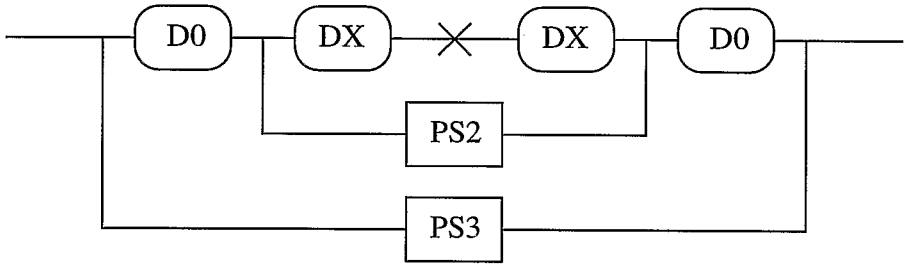

BLUE ring DX and D0 shunts

Figure 2: DX and D0 power supply shunts (except 10:00).

2.1 Inside the dipole pair

Since the second magnet in a DX or D0 pair bends in the opposite direction to its mate, the downstream dipole of a pair will have an error of $-\Delta x'$. The total angular displacement at the enclosed IP is therefore

$$x'^* \approx -\Delta x' \sqrt{\frac{\beta_D}{\beta^*}} \cot(\pi Q) \tag{6}$$

Since there are no quadrupoles between the IP and a DX or D0 magnet, then

$$\beta_D \approx \frac{s_D^2}{\beta^*} \tag{7}$$

where s_D is the distance from the IP to the dipole. If the dipole error is a fraction r of the whole, the angular perturbation is

$$\Delta x' = r\,\theta_D \tag{8}$$

The natural angle of the beam is

$$\sigma'^* = \sqrt{\frac{\epsilon_N}{6\pi(\beta\gamma)\beta^*}} \tag{9}$$

Putting these last four equations together to compare the closed orbit perturbation with the natural angle of the beam gives

$$\frac{x'^*}{\sigma'^*_{20}} \approx -r\,\frac{s_D\theta_D}{\sigma^*_{20}}\,\cot(\pi Q) \tag{10}$$

where the subscript "20" signifies that a standard normalized emittance of $\epsilon_N = 20\ \pi\mu$m is assumed from here on. To put it more succinctly,

$$\frac{x'^*}{\sigma'^*_{20}} = -\frac{r}{r_D}\,\cot(\pi Q) \tag{11}$$

where the "reference error"

$$r_D \equiv \frac{\sigma^*_{20}}{s_D\theta_D} \tag{12}$$

scales like $\sqrt{\epsilon_N\beta^*}$, and is independent of tune. Note that $\cot(\pi Q) \approx 1.47$ for the nominal fractional tune of $Q = .19$.

Quantity	Symbol	Units	Proton inject	Proton store	Gold inject	Gold store
Beta function	β^*	[m]	10.0	1.0	10.0	1.0
RMS bunch size	σ^*_{20}	[mm]	1.03	0.11	1.63	0.18
RMS bunch length	σ_z	[m]	.353	.072	.467	.206
RMS bunch angle	σ'^*_{20}	[mrad]	0.10	0.11	0.16	0.18
Aspect angle	θ_z	[mrad]	2.92	1.53	3.49	0.87
DX reference error	r_{DX}	$[10^{-3}]$	4.69	0.50	7.42	0.82
D0 reference error	r_{D0}	$[10^{-3}]$	3.04	0.32	4.81	0.53

Table 4: DX and D0 common mode error parameters.

Table 4 can be used to gauge whether an error - for example, a power supply regulation error - is big or not. If $r = r_D$, then there is a pure angle error of $x'^* = 1.47\sigma'^*$ at the IP inside the dipole pair. This is much less dangerous than a displacement error equal to the beam size at the IP, $x^* = \sigma^*$, which would not only lead to a large luminosity loss, but would also drive strong odd beam-beam resonances. A pure angle error only becomes similarly threatening when it is about as large as the aspect ratio angle

$$\theta_z \equiv \frac{\sigma^*}{\sigma_z} \tag{13}$$

where σ_z is the RMS bunch length. Table 4 shows that θ_z is typically an order of magnitude larger than σ'^*_{20}, showing that, so far as effects *inside* the dipole pair are concerned, common mode dipole errors as large as $r \approx r_D$ are tolerable. The situation in the rest of the ring, *outside* the dipole pair, is not so benign.

2.2 Outside the dipole pair

Outside the dipole pair, the total effect is given simply by multiplying equation 3 by 2, to give

$$x = \Delta x' \sqrt{\beta_D \beta}\, \frac{\cos(|\Delta\phi| - \pi Q)}{\sin(\pi Q)} \tag{14}$$

$$= a_x \cos(|\Delta\phi| - \pi Q) \tag{15}$$

where $\Delta\phi$ is the phase advance measured from the first dipole. The quantity of concern here is a_x, the closed orbit wave amplitude. Comparing it with the beam size and proceeding as before, it is easy to show that, at an arbitrary location,

$$\frac{a_x}{\sigma_{20}} = \frac{r}{r_D} \frac{1}{\sin(\pi Q)} \tag{16}$$

Except for the numerical factor $1/\sin(\pi Q) \approx 1.78$, this equation is almost identical in form to equation 11.

If the phase advance from the dipole pair is unfortunate, an error of $r = r_D$ can produce an unacceptable closed orbit shift of order σ_{20} at a remote IP. While "slow" transfer function and setting errors of order r_D can be observed and removed by closed orbit correction, "fast" regulation (ripple) errors at this level must be avoided. Crudely speaking, since 6 pairs of each kind of dipole affect each ring, it is necessary to ensure that the total current in each DX and D0 pair is correct at the level

$$r \ll \frac{r_D}{\sqrt{6}} \tag{17}$$

where $\ll$ implies an order of magnitude reduction, and the r_D values are those listed in Table 4. However, since r_D varies like $\sqrt{\beta^*}$ from one IP to the next, the tightest regulation need only be applied at IPs with the smallest β^* values. At least at some locations the ripple must be held below 10^{-5}, corresponding to .05 A out of a total of 5 kA.

3 Closed orbit correction strategy

It is a common practice in existing accelerators to occasionally remove an average offset in horizontal arc dipole correctors by adjusting the main arc dipole supply. Similarly, in RHIC, dipole correctors can be used to trade-off with DX and D0 magnets in each IR. This is complicated by the fact that the optimal strengths of three magnet pairs - DX, D0(Blue), and D0(Yellow) - are interrelated. Before returning to discus this two ring coupling further, first assume that the closed orbit in one ring is to be corrected with no consideration for the other ring. This might be the case, for example, when single ring injection is being tuned up.

The controls application *Orbit* will measure the closed orbit in a single ring by reading Beam Position Monitors (BPMs), before adjusting the dipole correctors to move the closed orbit closer to the goal trajectory. *Orbit* will be able to do this globally, or locally - for example, at a single IR. The hysteresis backlash on the DX and D0 dipoles is much larger than in dipole correctors, so that their routine adjustment is discouraged. Hence, in routine operation *Orbit* will not adjust any of the main dipole power supply strengths - neither the arc dipoles, nor the DX or D0 magnets.

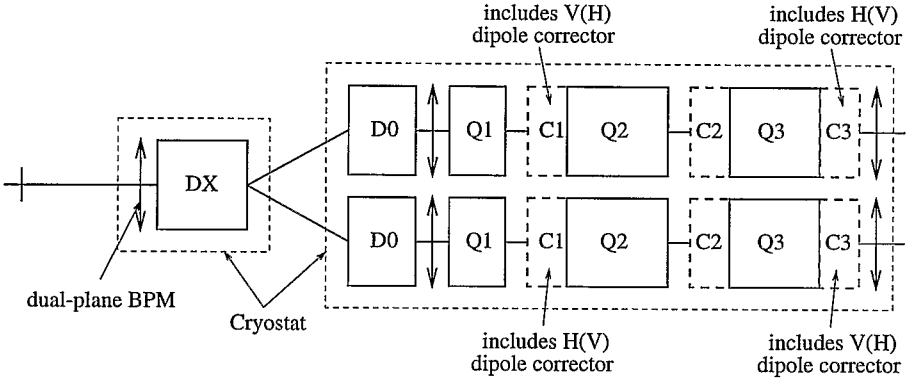

Figure 3: Schematic layout of Beam Position Monitors and dipole correctors.

Figure 3 shows that each IR has two dual plane BPMs in between each pair of DX magnets, which independently measure the angle and displacement of each beam. Since crossing angle adjustment is a specialized activity, and since it is conceptually useful to decouple the two closed orbits, it is desirable for *Orbit* to leave the horizontal crossing angle untouched in routine operation. Thus it may be appropriate to impose a "horizontal crossing angle override" on the horizontal goal values in the two inner BPMs, so that their difference maintains a constant value during repeated *Orbit* corrections. Such an implementation would not interfere with horizontal displacement corrections at the IP.

After the two closed orbits have been independently corrected in this fashion, the largest remaining errors will be in DX, D0(Blue), and D0(Yellow) pairs at each IP. Insofar as a D0 pair in one ring is not properly matched with its nearby DX pair (deviating from equations 1 and 2), there will be a closed orbit disturbance outside the D0 pair. This disturbance will be damped in about one betatron period by the closed orbit correctors, to disappear well before it reaches the neighboring IRs. Since it is easy for *Orbit* to calculate the dipole corrector response to a D0 pair error, it is also easy to invert this problem, calculating the required change in D0 strength to properly match the DX pair.

When D0 pairs in both rings at a single IP have been corrected in this way, all three DX and D0 pairs are simultaneously tuned in accordance with equations 1 and 2, to adjust the difference mode crossing angle to its desired value. Closed orbit differences should only be visible to the inner pair of BPMs during this operation. It may still be necessary to independently correct a common mode horizontal crossing angle in each ring. If so, the "horizontal crossing angle override" applied to the inner BPMs needs to be temporarily removed.

4 Vernier scans

Precise orbit control is required at each IP in order to optimize the luminosity, and to calibrate the luminosity monitors with high accuracy. This includes localized control of both the displacement and the slope of the closed orbit.

A complete analysis of luminosity monitor calibration must consider multiple bunches with differing populations and sizes, non-Gaussian bunches, and longitudinal issues such as crossing angles and the "hourglass" effect [6, 7, 8, 9]. However, since the emphasis here is on the implementation of local displacement bumps to perform horizontal and vertical "Vernier scans" at a single IP, it is appropriate to adopt a simple collision scenario. Assume, therefore, that there is only a single Gaussian bunch in each beam, and that longitudinal effects can be ignored ($\beta^* \gg \sigma_z$, $\alpha = 0$, et cetera). In this case the luminosity is given by

$$L = \frac{f N_B N_Y}{4\pi\sigma_H\sigma_V} \times \exp\left\{-\frac{1}{2}\left[\frac{\Delta x^2}{2\sigma_H^2} + \frac{\Delta y^2}{2\sigma_V^2}\right]\right\} \tag{18}$$

where f is the revolution frequency, N_B and N_Y are the bunch populations, and the beam size parameters σ_H and σ_V are derived from different size Blue and Yellow bunches through

$$\sigma_H = \sqrt{0.5(\sigma_{BH}^2 + \sigma_{YH}^2)} \tag{19}$$

$$\sigma_V = \sqrt{0.5(\sigma_{BV}^2 + \sigma_{YV}^2)} \tag{20}$$

The parameters Δx and Δy represent horizontal and vertical collision displacements. For example, a relative offset of $\Delta_x = 0.5\sigma_H$ leads to a 6% luminosity reduction.

The beam sizes σ_H and σ_V may be measured by making *relative* luminosity measurements during a Vernier scan of the collision displacements Δx and Δy [?]. Then, if N_B and N_Y are accurately known, Equation 18 leads directly to an absolute calibration of the luminosity monitor. Thus, the absolute calibration of each luminosity monitor is possible given only the availability of:

1. accurate measurements of the single bunch populations, N_B and N_Y
2. accurate local displacement bumps at each IP.

Current measurements of the single bunch populations N_B and N_Y using a DCCT are expected to have errors of less than 1%, provided that unwanted beam (in other buckets, or unbunched) is carefully removed. Therefore, it is likely that (preliminary) efforts to calibrate the luminosity monitors will be limited by the calibration accuracy of localized closed orbit bumps at the IPs.

4.1 Displacement and angle 4-bumps

Since the horizontal and vertical bumps used for Vernier scanning should not introduce a crossing angle, they should be "displacement 4-bumps", using four dipole correctors. With different relative strengths, the same four correctors can also create "angle 4-bumps" which do not modify the displacement at the IP. Two of the 4-bump correctors are in the triplets - each triplet contains one horizontal and one vertical dipole corrector, as shown in Figure 3. The outer two 4-bump correctors are near the Q4 quadrupole on one side of the IP, and near the Q5 quadrupole on the other side. Dipole correctors in the triplet have an ID of 13 cm, while those at Q4 and Q5 have an ID of 8 cm.

It is relatively straightforward to derive the ratios of the four dipole corrector strengths, in the absence of optical errors. Because of the anti-symmetry of the IR optics, the same set of corrector ratios works for both vertical and horizontal 4-bumps of the same kind. The correctors to be used for a bump in a given plane (horizontal or vertical) are located near quadrupoles which focus in that plane. The corrector strengths necessary to create a 1 mm displacement 4-bump at the top RHIC energy ($B\rho = 839.5$ Tm) at an IP with $\beta^* = 1$ m and 10 m are given in Table 5. Similarly, the corrector strengths for a 0.1 mrad angle 4-bump are given in Table 6. The displacement and angle 4-bumps themselves are shown in Figures 4 and 5 for $\beta^* = 1$ m. There is little difference in the $\beta^* = 10$ m case. The maximum field integral measured in *both* 13 cm and 8 cm correctors at 50 A is about 0.281 Tm, corresponding to a maximum angle of 0.335 mrad [10]. The largest displacement bump at top energy is therefore 9.4 mm, and the largest angle bump is 0.43 mrad.

It is a demanding task to step a displacement bump in precise increments which are much less than the beam size, in order to calibrate the luminosity monitors during a Vernier scan. Accurate estimations of the possible sources of beam orbit error are necessary.

corr.	$\beta^* = 1m$		
	Kick (10^{-6} rad)	Integral (10^{-3} Tm)	Current (A)
Q5	8.14	6.834	1.199
Q3	25.85	21.701	3.807
Q2	35.38	29.701	5.211
Q4	28.15	23.632	4.146

corr.	$\beta^* = 10m$		
	Kick (10^{-6} rad)	Integral (10^{-3} Tm)	Current (A)
Q5	10.72	8.999	1.579
Q3	22.85	19.183	3.365
Q2	35.50	29.802	5.228
Q4	24.70	20.736	3.638

Table 5: Corrector strengths for a 1 mm displacement 4-bump, when $\beta^* = 1$ m (top) and when $\beta^* = 10$ m (bottom).

corr.	$\beta^* = 1m$		
	Kick (10^{-6} rad)	Integral (10^{-3} Tm)	Current (A)
Q5	-33.55	29.844	-5.236
Q3	8.46	7.102	1.246
Q2	11.84	9.940	1.744
Q4	77.96	65.447	11.482

corr.	$\beta^* = 10m$		
	Kick (10^{-6} rad)	Integral (10^{-3} Tm)	Current (A)
Q5	-43.68	36.669	-6.433
Q3	18.17	15.254	2.676
Q2	11.79	9.898	1.736
Q4	68.46	57.472	10.083

Table 6: Corrector strengths for a 0.1 mrad angle 4-bump, when $\beta^* = 1$ m (top) and when $\beta^* = 10$ m (bottom).

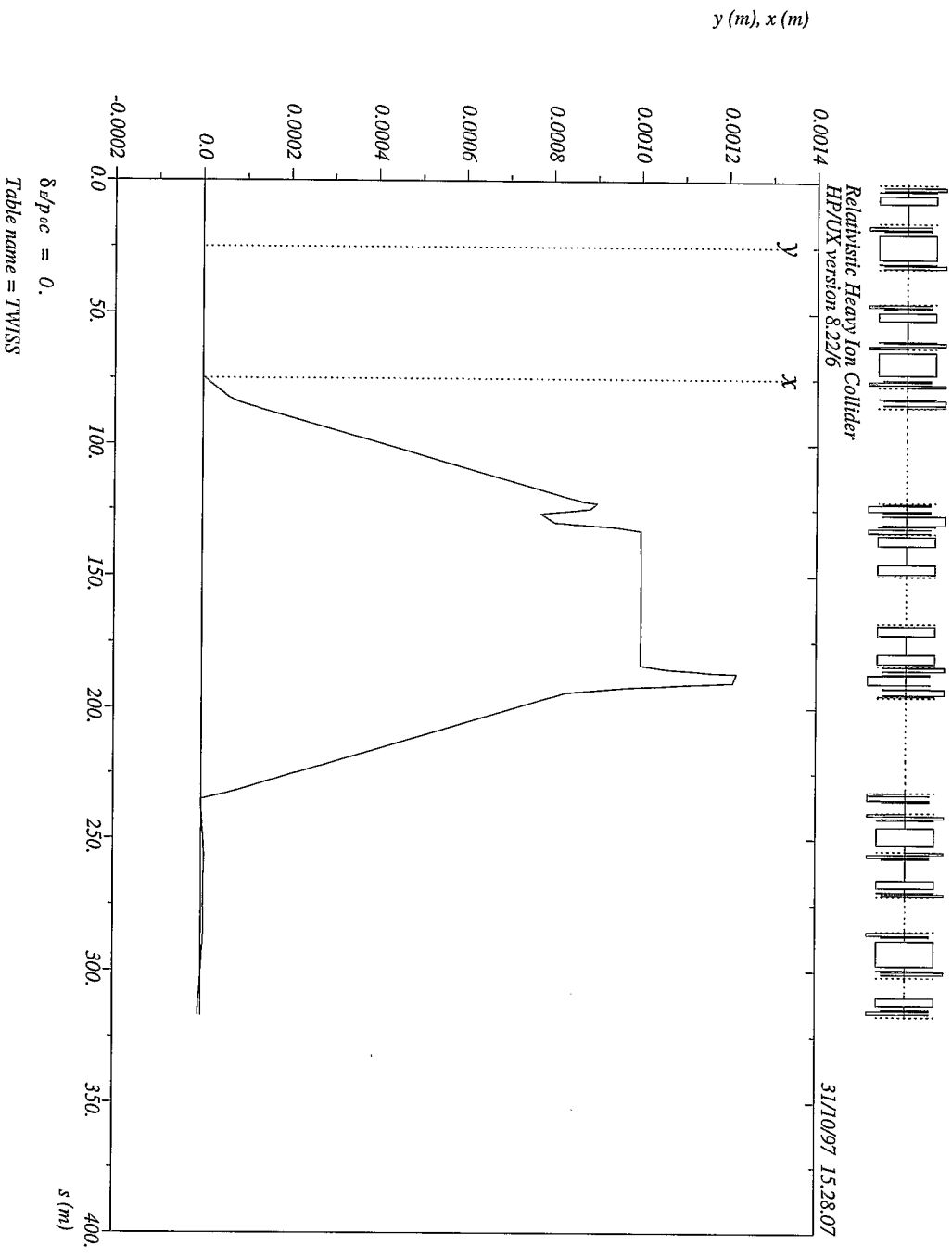

Figure 4: A 1mm displacement 4-bump at a single interaction point.

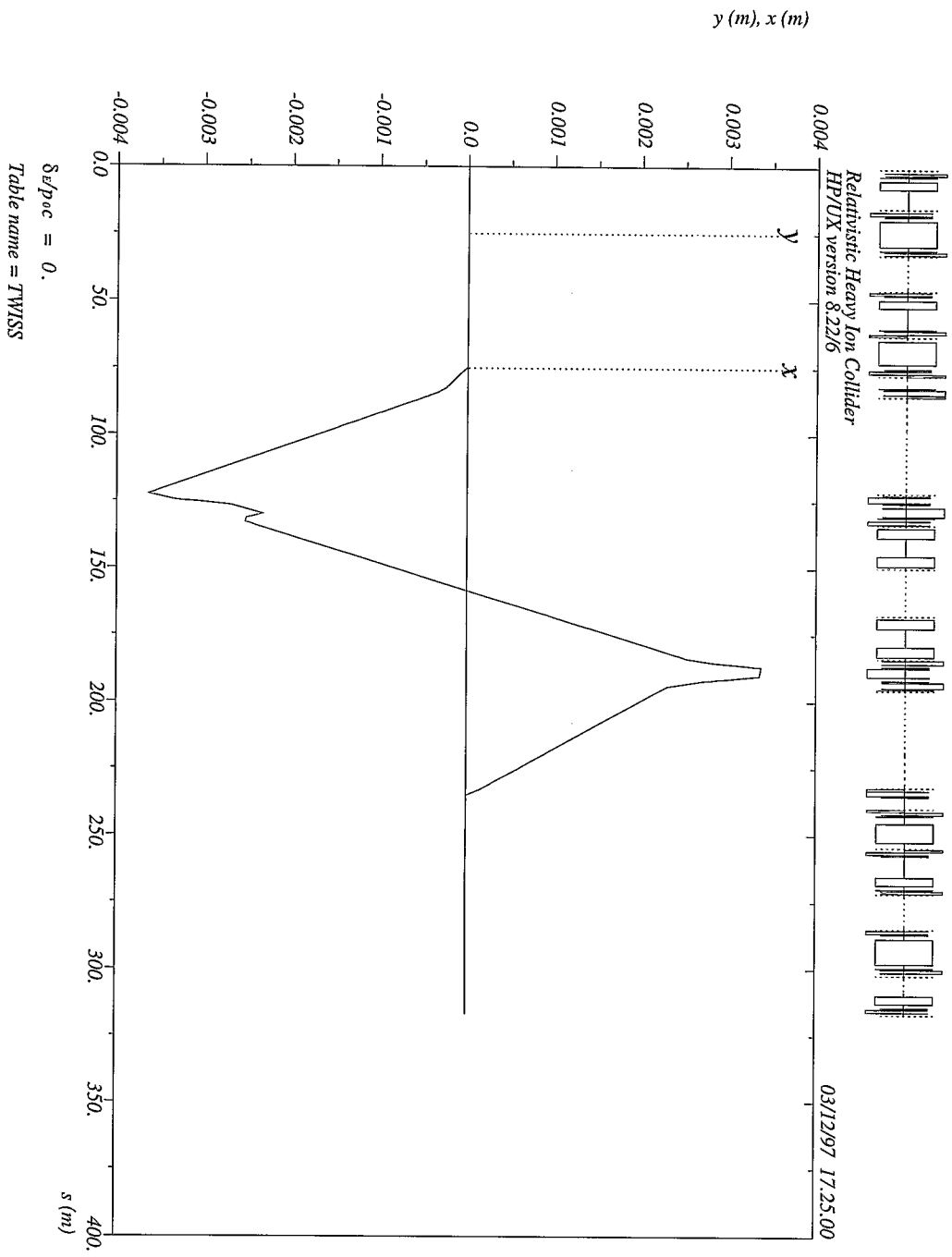

Figure 5: A 0.1 mrad 4-bump at a single interaction point.

In practice it will be necessary to adjust the 4-bump corrector strength ratios empirically in order to ensure that the closed orbit perturbation is indeed localized, and to ensure that no crossing angle is generated by the displacement 4-bump, and vice versa. Note that all of these constraints are null conditions - it is not necessary to depend on absolute BPM calibration. When the 4-bumps have been closed empirically, calibration uncertainties and errors depend *only* on optical errors *inside* the 4-bump. Although optical errors come in principle from uncertainties in both geometry and strength, in practice only the strength errors are a concern.

5 IR dipole corrector transfer function

The transfer function of a dipole corrector is the integrated field divided by the excitation current:

$$\kappa = \frac{\int Bdl}{I} \tag{21}$$

Note that this is *not* the derivative of the field integral with respect to current, a quantity with the same dimensions that is used by some authors.

Two problems arise in using measured transfer functions to make an absolute determination of beam motion:

1. Magnet to magnet variation in transfer function
2. Hysteresis through field variations produced by superconductor magnetization.

The transfer functions of all 13 cm dipole correctors are being measured warm (at low current), but not all are being measured cold. Individual information will be embedded by the *ramp manager* in the Wave Form Generator card that controls each IR dipole corrector power supply. For those correctors only measured warm, this will require the "warm-to-cold" correlation of transfer functions. In practice this is accurate enough to capture most of the individual characteristics of a particular dipole corrector.

5.1 Transfer function variation

Fig. 6 shows the variation of dipole transfer functions at a current of 30 A for all the 13 cm correctors that have so far been measured cold. There is no apparent difference between different model types. Fig. 7 shows a histogram of these values. The mean transfer function at an excitation of 30 A is 56.24 Gm/A, with a standard deviation of 0.15 Gm/A.

From Table 7, it appears that the variation in transfer function measurements is larger for lower currents. What is actually being seen is the approximately constant field uncertainty due to superconductor magnetization being

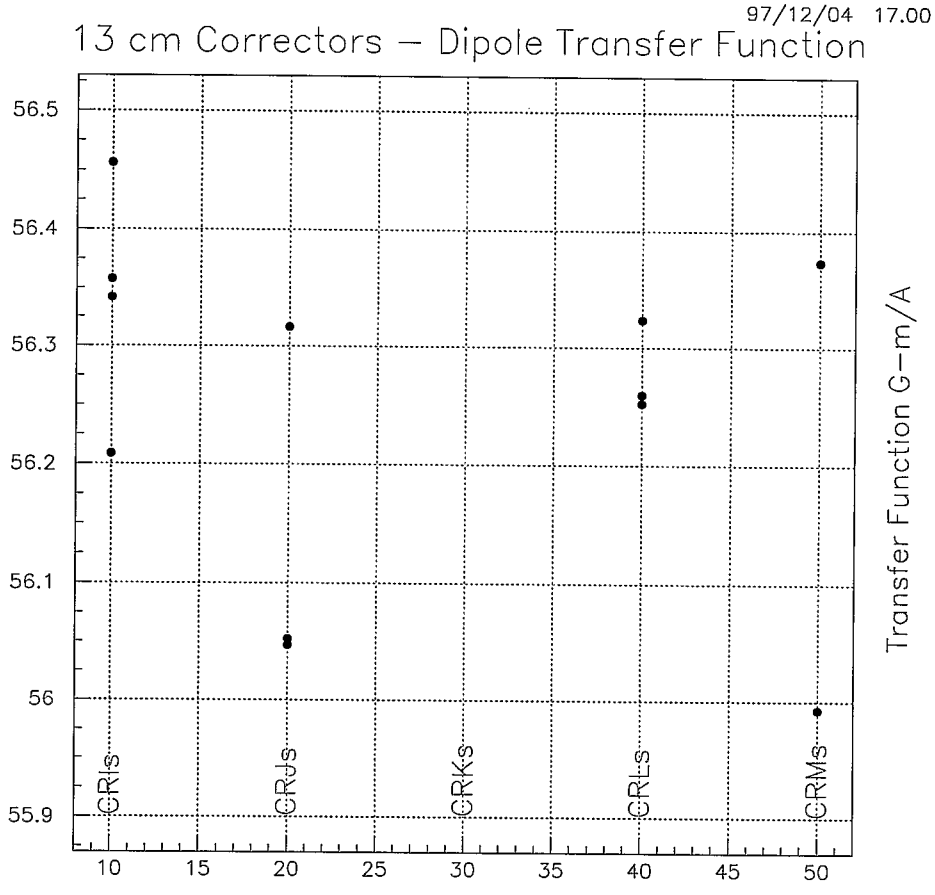

Figure 6: Transfer function data for the 5 different models of 13 cm dipole correctors, at 30 Amps.

divided by a smaller current. If one uses the average value of the transfer function for a specific magnet, one introduces an uncertainty of ~ 0.2 Gm/A. This is due mainly to uncertainties in the magnetization history rather than to errors in the measurement technique.

5.2 Superconductor magnetization

In a Type II superconductor, with a transport current less than short sample, a magnetization current is induced by any change in magnetic field. This is a change produced effect. It is *not* the Meisner Effect seen in Type I superconductors. Further changes in the field do not erase these currents but rather add new ones until the total of transport current and magnetization currents

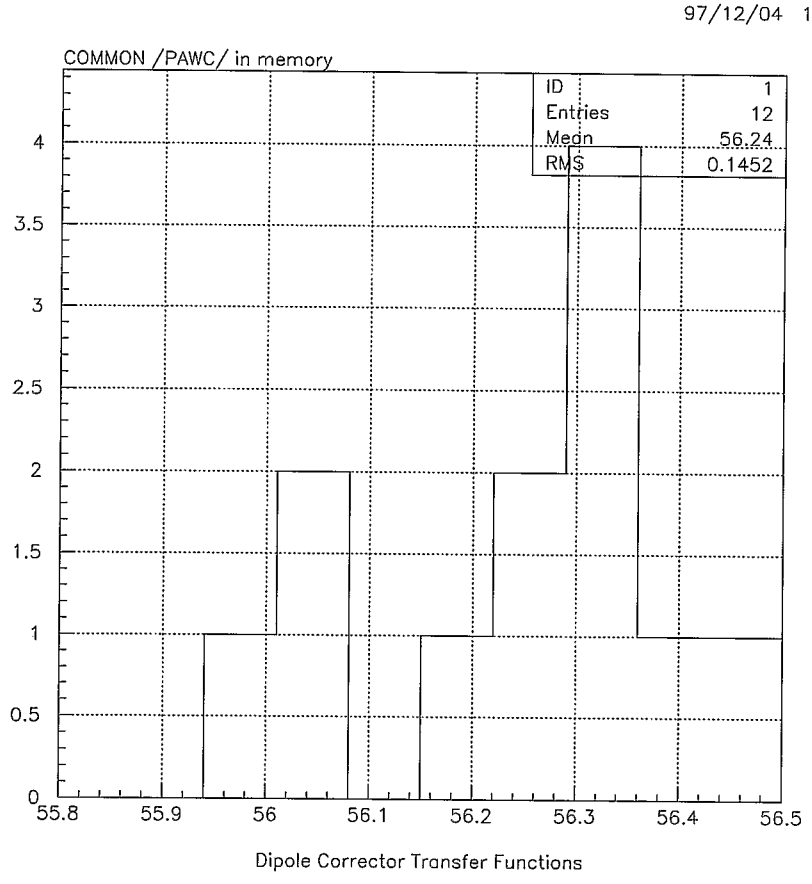

Figure 7: A histogram of transfer function data for all 13 cm dipole correctors, at 30 Amps.

equals the short sample current. The conductor thus retains a memory of field changes. This memory may be cleared by increasing the transport current to short sample (impossible to do throughout a magnet) or warming the conductor above T_c.

In measuring the field integral produced by the dipole correctors a "virgin" magnet is ramped up to +70 A, taking measurements in 10 amp increments. The magnet is then ramped back down to −70 A and back to 0 A. Normally only one such cycle is measured. Fig. 8 shows the transfer function variation around such a cycle. The effects of magnetization are better understood by plotting the field integral versus current, as shown in Fig. 9. For clarity, we subtract a linear field integral (in current) of 56.170 Gm/A. Immediately apparent in this figure is the $\sim$ 3 Gm hysteresis produced by history dependent fields. Reversing the

Current [A]	Transfer Function [Gm/A]
10	56.09 ± 0.390
-10	56.33 ± 0.361
20	56.21 ± 0.203
-20	56.33 ± 0.191
30	56.24 ± 0.140
-30	56.33 ± 0.143
40	56.26 ± 0.108
-40	56.32 ± 0.120
50	56.26 ± 0.090
-50	56.31 ± 0.109
60	56.25 ± 0.079
-60	56.29 ± 0.105

Table 7: Transfer function statistics for 13 cm dipole correctors.

direction of current change can result in a field integral offset of this amount. For practical currents (less than 50 A) this effect is approximately constant. The relative effect of hysteresis is minimized by running at the highest possible current, and sweeping in only one direction.

Further inspection of Fig. 9 reveals an average vertical offset of 2 Gm. If cycling is continued, the whole pattern may "walk" down by part of this amount on cycle 2, and a smaller amount on cycle 3, et cetera. This process does converge. Without the capability to run the coil at much higher currents (approximately 120 A) there is an uncertainty of $\sim$ 2 Gm in the field integral at a given current, in addition to the hysteresis spread of $\sim$ 3 Gm. At the time of writing it has not been determined how data such as those in Fig. 9 will be represented in the Wave Form Generator card, except that it will be possible to include multiple transfer function values at multiple excitations. Hysteresis will not be modeled.

For present purposes it is reasonable to assume a maximum absolute error of $\sim$ 3 Gm, corresponding to an angle of $\sim$ 0.36 μrad at top energy, to be compared with the 50 A maximum of 335 μrad. The differential field errors produced during a unidirectional sweep are much smaller than this. A reasonable estimate for the uncertainty in the change in field integral, working in the region 10-30 A and given perfect knowledge of the current, is less than 0.4 Gm. This corresponds to an angle of 0.048 μrad at storage.

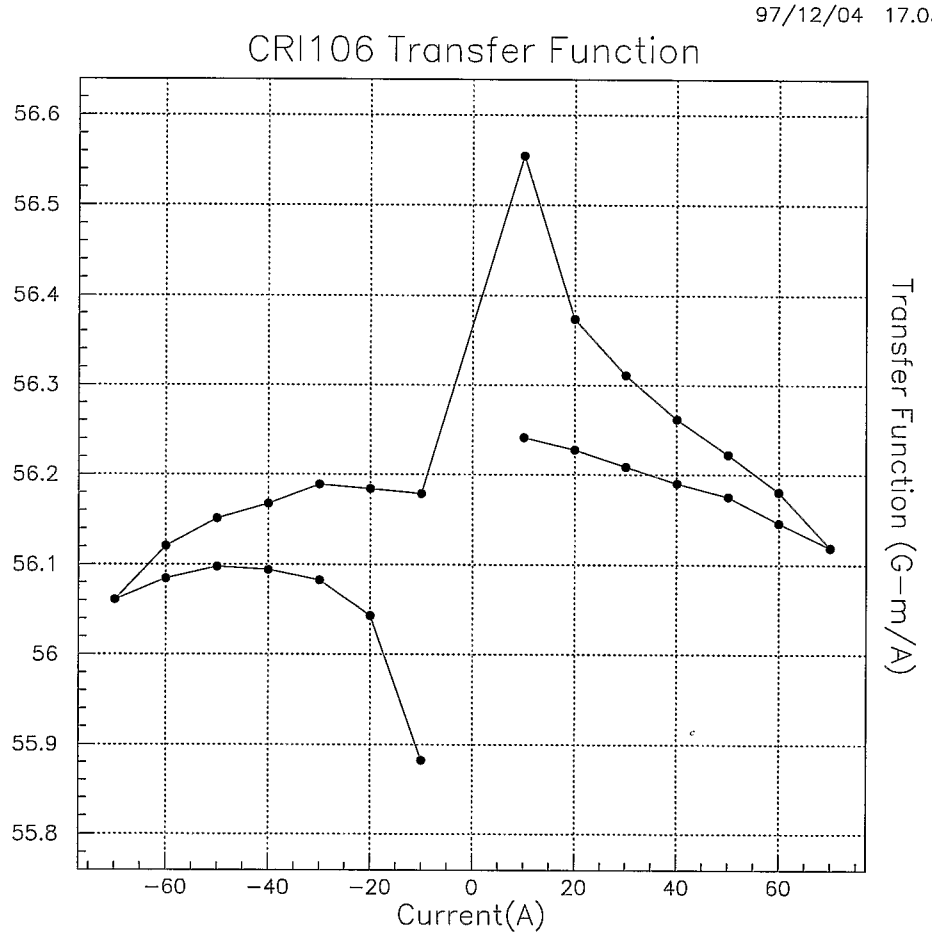

Figure 8: Transfer function variation of a typical 13 cm dipole corrector around a hysteresis loop, from 0 A to +70 A, then to −70 A, and back to 0 A.

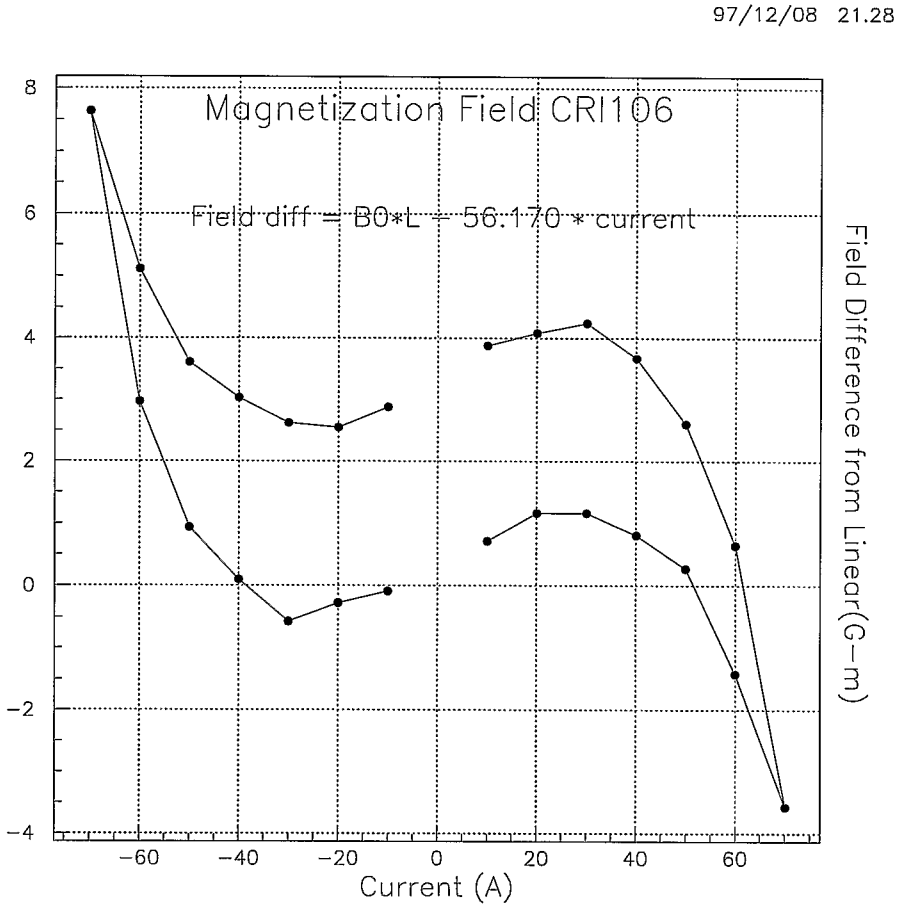

Figure 9: Field integral versus current (hysteresis loop) for a typical 13 cm dipole corrector, after subtracting a term linear in current.

5.3 Summary

1. The basic uncertainty in the transfer function is $\delta\kappa \approx 0.1$ Gm/A. This is the approximate value that applies to both hysteresis effects in a single magnet, and to the variation across the dipole corrector population, at 30 A.

2. Accurate sweeps *must* be unidirectional. If possible, it is highly desirable to "reset" each magnet by running the current up and down through a standard loop between sweeps.

3. The absolute field integral error is less than 3 Gm, or 0.36 μrad at storage. The uncertainty in the differential field integral produced during a unidirectional sweep is less than 0.4 Gm, or 0.048 μrad.

4. Further measurements of the differential field integral are desirable, under these conditions.

5. Bench measurements of the transfer function of the dipole layer of a 13 cm corrector are usually made with the other corrector layers *off*. The transfer function will in general be larger with the other layers powered. Again, further measurements are desirable to better determine the size of this effect, which could be significant.

6 Orbit bump errors

First let us estimate the errors coming from the dipole correctors used in the displacement bump. These are due to:

1. transfer function errors

2. uncertainties in the current provided by the power supplies.

Assume that the 4-bump ratios have been empirically adjusted to ensure that the closed orbit perturbation is localized, but that each corrector i still has a residual independent relative strength error ϵ_i', so that the net angular kicks are

$$\Delta x_i' = \Delta x_{0i}'(1+\epsilon_i') \tag{22}$$

These errors lead to a total IP displacement error of δx^*, where

$$\delta x^* = \sqrt{\beta^*}\sum_i K_i \Delta x_{0i}' \epsilon_i' \tag{23}$$

The response coefficients K_i are defined by

$$K_i = \sqrt{\beta_i}\,\frac{\cos(|\Delta\phi_i| - \pi Q)}{2\sin(\pi Q)} \tag{24}$$

where $\Delta\phi_i$ is the betatron phase advance between the IP and the i-th corrector. The response coefficients K_i are considerably larger for the correctors near Q2 and Q3 quadrupoles which are in the high beta region, than for the correctors near Q4 and Q5 quads. In consequence, the orbit errors caused by these correctors are considerably larger. If the bump amplitude in the absence of the corrector errors ($\epsilon_i' = 0$) is Δx^*, the relative displacement error

$$\epsilon_x \;=\; \delta x^*/\Delta x^* \tag{25}$$

due to a single error $\epsilon_i' = 1\%$ in the i-th corrector is given in Table 8.

Corrector	$\epsilon_x(\%)$
Q5	0.02
Q3	0.49
Q2	0.59
Q4	-0.10

Table 8: The relative orbit error due to a single uncorrected 1% error in one displacement bump dipole corrector.

In the case of four random uncorrected errors, with an RMS strength

$$\sigma_\epsilon \;=\; <\epsilon'^2>^{1/2} \tag{26}$$

the net RMS displacement error is

$$\epsilon_x \;=\; \frac{\sigma_\epsilon\sqrt{\sum_i (K_i\Delta x_{0i}')^2}}{\sum_i K_i\Delta x_{0i}'} \;\approx\; \frac{\sigma_\epsilon}{\sqrt{2}} \tag{27}$$

where the approximation reflects the fact that the two IP high-beta correctors generate most of the total error.

As discussed in section 5, the largest absolute uncertainty in the transfer function comes from uncertainties in the magnetization history of each individual corrector, that is from hysteresis, rather than from measurement errors. This absolute uncertainty is at the level of $\delta\kappa \approx 0.1$ Gm/A, while the transfer function itself is about $\kappa \approx 56$ Gm/A. If no attention is being paid to the unidirectionality of the dipole corrector excitation, and the excitation is about 30 A, one expects the RMS strength error to be

$$\sigma_\epsilon \;\approx\; \frac{\delta\kappa}{\kappa} \;\approx 0.2\% \tag{28}$$

Since the relative displacement error is of order σ_ϵ, dipole corrector hysteresis appears to be of little importance in routine orbit tuning.

6.1 Power supply current uncertainty

When a unidirectional Vernier scan is performed with perfect knowledge of the excitation current, the uncertainty in the change of the field integral corresponds to an angle of less than 0.048 μrad at top energy, according to section 5. Unfortunately this perfect knowledge is not practically attainable, and the main contribution to 4-bump displacement errors during incremental Vernier scanning comes from the uncertainty of the power supply current.

In the best case, the use of 12 bit DACs in the ± 50 A corrector power supplies leads to an RMS current uncertainty of $\sigma_I = 100/(2^{11} \cdot \sqrt{12}) = 14.1$ mA, corresponding to a dipole corrector angular uncertainty of 0.095μrad at top energy. Suppose that we want to use Vernier scan steps of $\sigma/3$, about 40 μm when $\beta^* = 1$ m and the gold emittance is 40 $\pi\mu$m at top energy. In this case the current uncertainty leads to $\epsilon \approx 8\%$, and using (27) the uncertainty of the displacement step becomes $\epsilon_x \approx 6\%$.

This is the best possible case. At lower operating energies we need to scan the corrector currents with even smaller steps, and the orbit error grows as $1/\sqrt{\gamma}$. All this argues in favor of decreasing the current uncertainties by using DACs with 14 or 16 bits.

6.2 Triplet quad errors

To estimate the influence of insertion quadrupole errors on orbit control at the IP we use the closed orbit equation

$$x'' + (k_0 + \delta k)(x - h) \;=\; g \tag{29}$$

where δk describes the error in the quadrupole focusing strength, h is the quad misalignment, and g represents the orbit corrector bending strength for both global orbit correction and for producing orbit bumps at the IP. All components are functions of the distance s along the ideal beam orbit. The solution of Equation 29 can be written

$$x \;=\; x_0 + \delta x \tag{30}$$

where x_0 is the deliberate closed orbit offset (for example, during a Vernier scan), and δx results from the quadrupole errors δk. If h or x_0 is large, and δk varies in time (during a Vernier scan, or since the last empirical 4-bump tuning), then significant values of δx can result.

Substituting Equation 30 into Equation 29 we obtain the following equation for δx

$$(\delta x)'' + (k_0 + \delta k)\delta x \;=\; -\delta k(x_0 - h) \tag{31}$$

The term $\delta k \delta x$ is much smaller than $k_0 \delta x$, and is dropped. Then one can see that quad errors can be considered as additional dipole kicks, with

$$\delta x'_q \;\equiv\; -\delta k_i (x_{0i} - h_i) L_i \tag{32}$$

where L_i is the length of the quadrupole. The orbit shift at the IP due to the quad errors is given by

$$\delta x^* \;=\; \sqrt{\beta^*} \sum_i K_i \delta x'_{qi} \tag{33}$$

using the same response coefficients K_i that were introduced in Equation 24

Again we are interested in estimating the relative orbit error $\epsilon_x = \delta x^*/\Delta x^*$ when producing small displacement 4-bumps with an amplitude of Δx^*. In this case we express ϵ_x through

$$\epsilon_x \;=\; \sum_i \omega_i \delta x'_{qi} \tag{34}$$

The largest error comes from the Q2 quad located at the highest β-function position, where both ω_i and r_i have their largest values. Assuming an orbit bump amplitude of $\Delta x^* = 40$ μm, we find for Q2 that

$$\omega \;\approx\; \frac{\sqrt{\beta^*}\sqrt{\beta_q}}{2\Delta x^*} \;\approx\; \frac{\sqrt{1300}}{2 \cdot 40} \;\mu\text{rad}^{-1} \;\approx\; 0.45 \;\mu\text{rad}^{-1} \tag{35}$$

The orbit deviation x_0 during Vernier scans is of the order of the beam size, so we can take $x_0 - h$ to be of the order of 100μm. The angular kick produced by the Q2 quad error is then

$$\delta x'_q \;\approx\; 19 \, \frac{\delta k}{k_0} \;\mu\text{rad} \tag{36}$$

and finally we have

$$\epsilon_x \;\approx\; 8.5 \, \frac{\delta k}{k_0} \tag{37}$$

Thus, to keep the orbit error at the 1% level one needs to keep the relative quadrupole error $\delta k/k_0$ below the level of $1.2 \cdot 10^{-3}$. Note that a 1% orbit displacement error corresponds here to an absolute orbit displacement of 0.4μm.

Taking into account a contribution to orbit displacement error from all 6 triplet quadrupoles having the RMS $\delta k/k_0$ error σ_k one can find

$$\epsilon_x \;\approx\; 13 \, \sigma_k \tag{38}$$

where again we assume $x_{0i} - h_i \approx 100\mu$m. According to this estimation $\sigma_k \approx 7.7 \cdot 10^{-4}$ for $\epsilon_x = 1\%$.

Quadrupole errors can come from power supply ripple or hysteresis errors. Note that if the relative quadrupole misalignment is small, $\Delta h \ll x_0 \approx 100\mu$m, there is a partial cancelation of orbit displacement error in IP due to the lattice antisymmetry about the interaction point. Also, one can estimate the contribution from a systematic error $\delta k/k_0$ as

$$\epsilon_x \;\approx\; 4.4 \, \frac{\delta k}{k_0} \tag{39}$$

References

[1] "Parasitic beam-beam collisions and crossing angles in RHIC", S. Peggs, RHIC/AP/66, August 1995.

[2] "Beam Sizes from Q4 to Q4 for Seven Different Operation Scenarios", S. Tepikian, RHIC/AP/85, February 1996.

[3] "Protons on gold at identical rigidities", S. Peggs, RHIC/AP/134, September 1997.

[4] For more information, try the public domain code *xgeom*, written and supported by S. Tepikian.

[5] "Magnet Electrical System", RHIC Design Manual.

[6] "Calibration of the Effective Beam Height in the ISR", S. van der Meer, ISR-PO/68-31, CERN, 1968.

[7] "Beam-Beam Interaction Effects in the Fermilab Collider", D. Siergiej, PhD Thesis, University of New Mexico, 1995.

[8] "Luminosity and beta function measurement at the electron-positron collider ring LEP", P. Castro-Garcia, Doctoral Thesis, University of Valencia, 1996.

[9] "Cogitations on luminosity", W. Mackay, RHIC/AP/??, to be published.

[10] One way is to simply fit a Gaussian to the data of relative luminosity counts versus position. There is also a more general method, reported by van der Meer, which works in two dimensions without any *a priori* assumptions about the beam distribution - even if it is not Gaussian. In this method (crudely speaking, in one dimension) the area measured under the "counts versus position" curve is divided by the maximum count.

[11] "RHIC Magnet Transfer Functions", F. Pilat, RHIC/AP/113, October 1996.